nanomaterials

MDPI

Article

Electrical Phase Control Based on Graphene Surface Plasmon Polaritons in Mid-infrared

Yindi Wang [1], Hongxia Liu [1,*], Shulong Wang [1,*], Ming Cai [1], Haifeng Zhang [2] and Yanbin Qiao [2]

[1] Key Laboratory for Wide Band Gap Semiconductor Materials and Devices of Education Ministry, School of Microelectronics, Xidian University, Xi'an 710071, China; wangyindi4213@126.com (Y.W.); cm9999787@163.com (M.C.)

[2] Beijing Smart-Chip Microelectronics Technology Co., Ltd. Beijing 100192, China; zzflys@163.com (H.Z.); wyd4213@163.com (Y.Q.)

* Correspondence: hxliu@mail.xidian.edu.cn (H.L.); slwang@xidian.edu.cn (S.W.); Tel.: +86-29-8820-4085 (H.L.); +86-15979166584 (S.W.)

Received: 7 February 2020; Accepted: 20 March 2020; Published: 22 March 2020

Abstract: Phase modulation of light is the core of many optoelectronic applications, such as electro-optic switch, sensors and modulators. Graphene Surface plasmon polaritons (SPPs) exhibit unique properties in phase modulation including dynamic tunability, a small driving voltage and small device size. In this paper, the novel phase modulation capability of graphene SPPs in mid-infrared are confirmed through theory and simulation. The results show that graphene SPPs can realize continuous tuning of the phase shift at multiple wavelengths in mid-infrared, covering the phase range from 0° to 360°. Based on these results, a sandwich waveguide structure of dielectric–graphene–dielectric with a device length of 800 nm is proposed, which shows up to 381° phase modulation range at an operating wavelength of 6.55 μm, given a 1 V driving voltage. In addition, the structure size is much shorter than the wavelength in mid-infrared and can realize sub-wavelength operation. This work paves the way to develop graphene-based tunable devices for mid-infrared wave-front control.

Keywords: grapheme surface plasmon polaritons; phase modulation; Mid-infrared

1. Introduction

Surface plasmon polaritons (SPPs), the electromagnetic waves coupled to charge excitations on the surface of metal, are widely applied in sub-wavelength-scale optical processing [1]. Because of the breakthrough of the diffraction limit and the ultra-compact mode confinement, SPPs have become the cornerstones of various applications, including optical metamaterials, ultra-sensitive optical biosensors [2–4] and quantum information processing [5]. In recent years, SPPs based on metals have been widely used, because most studies on SPPs focus on precious metals represented by silver and gold [4,6–9]. However, even noble metals, which are widely regarded as the best available SPPs materials, are hardly tunable. They also suffer large decoherence and exhibit large ohmic losses, which limit their application in light manipulation equipment. In this context, it is necessary to search for more excellent SPP materials to realize high tunability, lower transmission loss and stronger constraint [10].

Graphene, a monolayer of carbon atoms arranged in a honeycomb lattice [11], has been widely used in optical devices because of its excellent electro-optical performance [12–14]. Previous research on graphene has proven that this material is a zero-gap semiconductor and its chemical potential can be tuned dynamically [15], which can be doped to high values of carrier concentrations either electrically or chemically. These unique properties make graphene a potential material for tunable

optical devices such as modulators, polarizers, sensors, etc. Due to their tunability and small size, these graphene-based devices have advantages over traditional devices. In addition, graphene has been proven to support SPPs from a mid-infrared band to THz and SPPs bound to the surface of doped graphene, which exhibit a number of favorable properties [16,17]. The ability to fabricate large-sized, high-crystalline samples enables the lifetime of SPPs to reach hundreds of optical cycles, making graphene a potential alternative for precious metal SPPs [12].

The phase modulation of light is at the core of many applications and much research [18]. Phase modulation in mid-infrared can be applied to the design of a phased array radar, atmospheric communication equipment, mid-infrared detector, etc. [19,20]. It is a huge challenge to accomplish the design of these devices efficiently with a small device size [21]. However, traditional phase modulators in mid-infrared are mainly based on waveguides employing electro-optic materials such as GaAs and $LiNbO_3$, which have large device sizes and require high external driving voltages [22,23]. Besides, these phase modulators suffer relatively large power dissipation and weak tunability, which greatly limits their application in light manipulation equipment. In this context, graphene SPPs shows great potential in mid-infrared phase modulation, which exhibits unique properties as a phase modulation platform with dynamic tunability, small footprint and small drive voltage [21]. The carrier concentration of graphene can be tuned over a wide range by electrostatic gate [24,25]. However, at present, the study of mid-infrared phase modulation based on graphene is mostly confined to the regulation function of graphene, and the application of graphene SPPs in mid-infrared phase modulation has not been studied systematically. This paper theoretically demonstrates the phase modulation of mid-infrared light using electrically tunable graphene SPPs.

In this paper, we explore graphene SPPs phase modulation in mid-infrared by presenting a sandwich waveguide structure of dielectric–graphene–dielectric, which can realize phase modulation from 0° to 360° in situ. The structure length of 800 nm is much shorter than the free-space wavelength in mid-infrared, realizing sub-wavelength operation. Here, we provide a scattering theory for graphene SPPs' propagating and phase modulation through theoretical derivation and software simulation. The modulation is achieved by controlling the voltage applied to the graphene where the spatial carrier density is tunable. This work constitutes a first step for the application of graphene phase modulation in photoelectric devices such as ultracompact modulators and sensors.

2. Structure Design

Previous structural designs have employed metals directly patterned to graphene as gate electrodes [26–28]. Contact between graphene and metal has been proved to cause a Fermi level pinning effect [29,30]. This effect can severely restrict the modification range of graphene Fermi energy level, which weakens the phase modulation ability of graphene [31]. The graphene-based phase modulation structure proposed here avoids these deleterious effects. In addition, large contact resistance between the metal and graphene can also be avoided.

$HfAlO_x$ has the advantages of a low charge trap density and high mobility. It can contact graphene perfectly without destroying the carrier mobility of grapheme. As shown in Figure 1, the presented structure consists of a silicon or silicon-dioxide (SiO_2) substrate [32], 100 nm $HfAlO_x$ isolation layer, monolayer graphene, $HfAlO_x$ dielectric layer with a thickness of d, and a 50 nm thick gold electrode. Here, Chemical Vapor Deposition (CVD) is used to grow monolayer grapheme, and then can be transferred to $HfAlO_x$. As revealed in Figure 1a, the length of the structure is L, which is also the length of the optical path. In this structure, the $HfAlO_x$ dielectric layer serves as an effective high-k dielectric for graphene chemical potential tuning when external voltage (V_g) is applied between graphene and the metal gate. Here, the 100 nm $HfAlO_x$ isolation layer isolates graphene from the environment, which is conducive to maintaining the long-term stability of graphene and preventing the accumulation of substances adsorbed on graphene [30,33–35].

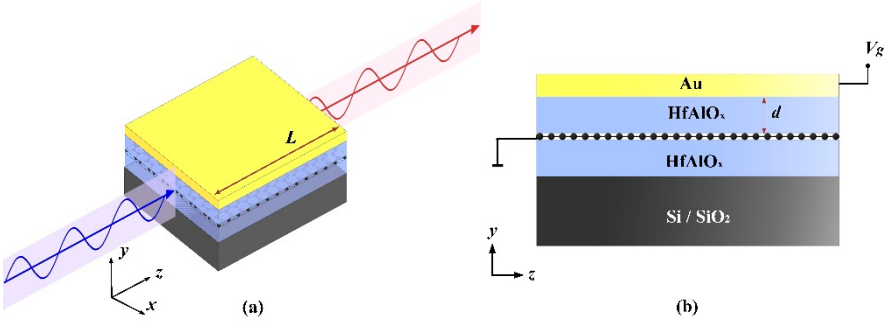

Figure 1. Schematic illustration of the proposed structure: (**a**) 3D layout; (**b**) cross-section.

3. Methods

Because SPPs are excited at the appropriate chemical potential, graphene has a strong response to mid-infrared electromagnetic waves [36]. In addition, the carrier concentration of graphene can be easily adjusted by electrostatic gating due to its atomic thickness and the linear density of electronic states [12]. For this proposed structure, the charge carrier density can be calculated with a parallel plate capacitor model [37]. The dielectric constant of graphene can be adjusted in a wide range [21]. The electrical phase control of graphene in mid-infrared band mainly depends on the electrical tunable carrier concentration and chemical potential of graphene.

Graphene can be considered as a two-dimensional material, and its surface conductivity σ is related to the radiation angular frequency ω, chemical potential μ, and relaxation time. The conductivity of monolayer graphene can be obtained from Kubo formula [10]

$$\sigma_{intra} = \sigma_0 \frac{4\mu}{\pi} \frac{1}{\hbar\tau_1 - i\hbar\omega} \tag{1}$$

$$\sigma'_{\text{inter}} = \sigma_0 \left(1 + \frac{1}{\pi}\arctan\frac{\hbar\omega - 2\mu}{\hbar\tau_2} - \frac{1}{\pi}\arctan\frac{\hbar\omega + 2\mu}{\hbar\tau_2}\right) \tag{2}$$

$$\sigma''_{inter} = -\sigma_0 \frac{1}{2\pi} \ln \frac{(2\mu + \hbar\omega)^2 + \hbar^2\tau_2^2}{(2\mu - \hbar\omega)^2 + \hbar^2\tau_2^2} \tag{3}$$

$$\sigma = \sigma_{intra} + \sigma'_{inter} + i\sigma''_{inter} \tag{4}$$

where τ_1 = 10 fs is the in-band relaxation time of graphene, and τ_2 = 1.2 ps is the inter-band relaxation time of graphene. $\sigma_0 = \pi e^2/2h$; $\hbar = 1.055 \times 10^{-34}$ J·s is the reduced Planck's constant.

By solving simultaneous Equations (1)–(4), the dependence of electrical conductivity on chemical potential of graphene will be obtained. Given a working wavelength 6550 nm, the relationship between graphene electrical conductivity and chemical potential is shown in Figure 2.

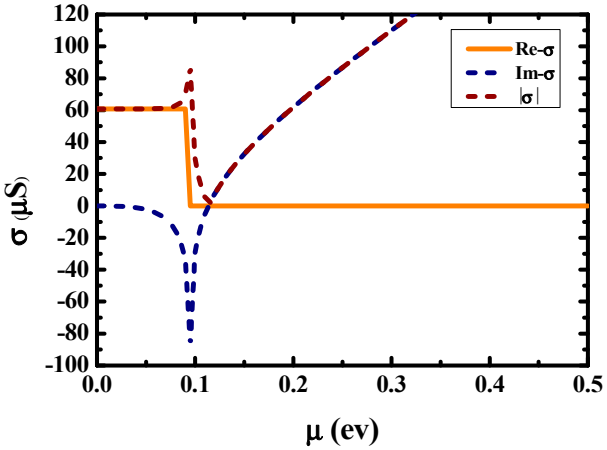

Figure 2. Dependence of conductivity on chemical potential.

The chemical potential of graphene can be tuned by external applied voltage [10]. The chemical potential of the graphene layer can be determined by the carrier concentration n_0

$$\mu = \hbar v_f \sqrt{\pi \cdot n_0} = \hbar v_f \sqrt{\pi \frac{\varepsilon_0 \varepsilon_r}{d \cdot e}(V_g + v_0)} \quad (5)$$

where $n_0 = \varepsilon_0.\varepsilon_r(v+v_0)/(d \cdot e)$. $v_f = 1.1\times10^6$ m/s is the Fermi velocity. v_0 is the offset voltage caused by natural doping, and its value is 0. ε_0 and ε_r are dielectric constant in free space and relative dielectric constant of the substrate material, respectively. d is the thickness of graphene substrate (the dielectric between gate and graphene), and V_g is the voltage applied to graphene.

Graphene in the proposed sandwich structure can be regarded as a layer of the current. By solving Maxwell equations and the boundary conditions of Maxwell equations, we can obtain the dispersion relation of SPPs wave in TM mode as shown in the following Equation (6) [10]

$$\frac{\varepsilon_1}{k_1} + \frac{\varepsilon_2}{k_2} + \frac{i\sigma}{\omega\varepsilon_0} = 0 \quad (6)$$

where k_1 and k_2 are P-wave vectors of the SPPs wave in upper and lower dielectric layers, respectively. The relationship between P-wave vectors and the propagation constant of SPPs (β) can be expressed as: ${k_m}^2 = \beta^2 - \varepsilon_m {k_0}^2$, where $m = 1, 2$. In the proposed structure, $\varepsilon_1 = \varepsilon_2 = \varepsilon_r$ (relative dielectric constant of $HfAlO_x$), and we can get the dispersion relation of graphene, as shown in Equation (7) [38]

$$\beta = k_0 \sqrt{\varepsilon_r - \left(\frac{2\varepsilon_r}{\eta_0 \sigma}\right)^2} \quad (7)$$

where k_0 is the propagation constant of electromagnetic waves in air. $\eta_0 = 377$ ohms is the impedance of free space.

Since the attenuation length of SPPs wave is much shorter than the thickness of the $HfAlO_x$ medium, it is not necessary to consider the spatial structure of the metal gate. From TM mode wave equation $H_x(y) = A_m e^{i\beta z} e^{-kmy}$, it can be seen that different phases ϕ are accumulated after propagation through different path lengths. The phase shifts $\Delta\phi$ in different optical transmission lengths can be calculated by optical path length L and the real part of β, which can be expressed as

$$\Delta\phi = \mathrm{Re}(\beta) \cdot \mathrm{L} \quad (8)$$

It can be obtained from the above equations that the propagation constant in transmission direction (β) can be tuned by different voltages applied to graphene and different thicknesses of $HfAlO_x$.

Thus, the phase shift of the graphene SPPs wave can be adjusted. The graphene SPPs phase shift is tunable in situ, and can be varied spatially, making it a unique platform for transformation optics in two dimensions

4. Results and Discussion

Through the discussions in the method section, we can conclude that the graphene SPPs phase shift is affected by a series of factors, including applied voltage (V_g), $HfAlO_x$ dielectric thickness (d), incident wavelength, the dielectric constant of the $HfAlO_x$ (ε_r) and optical path length (L). To further research the influence of all the factors on phase shift, the classical control variable method is adopted here. L is fixed at 800 nm in this structure, which can guarantee a completely adjustable phase shift from 0° to 360° in a voltage range of 5 V. In the simulations, the relative permittivities of Si and SiO_2 are 11.9 and 2.09, respectively [39–42].

The plots of the simulated phase shift ($\Delta\phi$) on incident wavelengths for different $HfAlO_x$ dielectric thickness (50, 100, 150, 200 nm) are shown in Figure 3a–d, respectively, incident wavelength is ranged from 2500 to 25,000 nm (mid-infrared region), and the dielectric constant of the $HfAlO_x$ used in this simulation is set at 14.3, which is in common use. As revealed in Figure 3, phase shift is selective to wavelength, and the maximum phase shift point shows blue-shift with increasing applied voltage, which is mainly because the tuned graphene conductivity resulted from the different applied voltage. The maximum phase shift shows nonlinear changes with different voltages. This depends on the nonlinear relationship between voltage and conductivity, conductivity and propagation constant. As revealed from the simulation results, phase shift of 360° can be reached at all wavelengths in mid-infrared band, by adjusting the applied voltage, substrate thickness and optical path length.

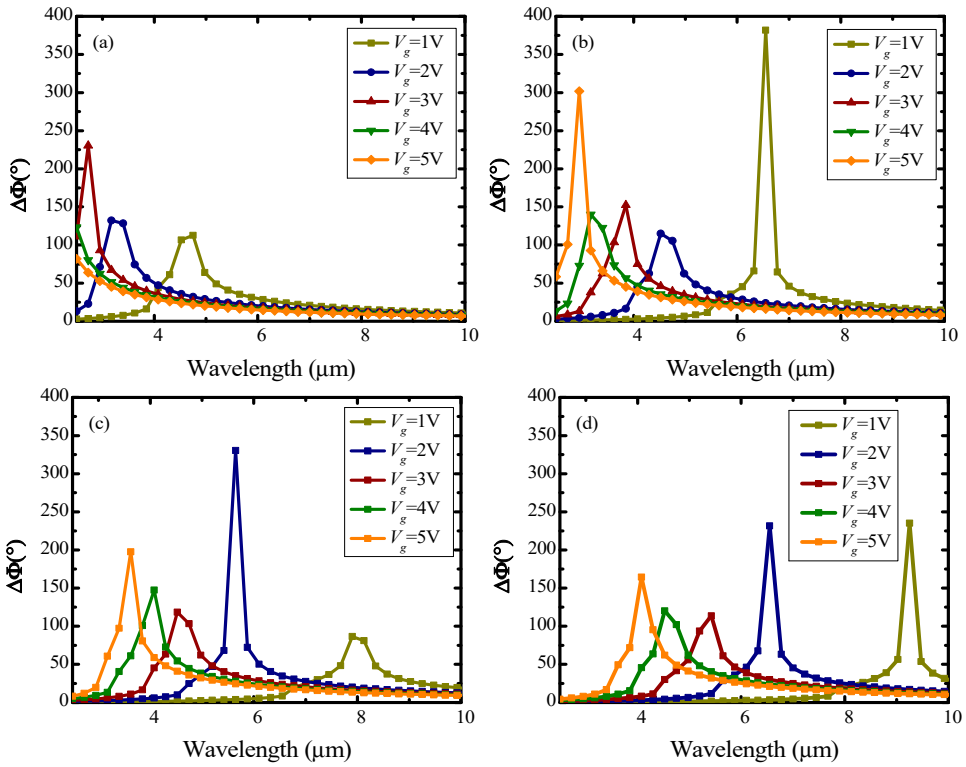

Figure 3. Dependence of phase shift on applied voltage and incident wavelengths at different $HfAlO_x$ dielectric thickness: (**a**) d = 50 nm; (**b**) d = 100 nm; (**c**) d = 150 nm; (**d**) d = 200 nm.

It can be obtained from Figure 3b that the phase shift reaches 381° at 6550 nm when d = 100 nm, V_g = 1 V. Next, fixing incident wavelength at 6550 nm, the influence of continuous applied voltage variation on phase shift is researched, as shown in Figure 4. As can be seen from Figure 4, the phase

shift peak (381°) appears at 1 V during the voltage variation, with a dielectric thickness of 100 nm. In this case, given a voltage ranging from 0 to 1 V applied to graphene, a phase modulation of 0° to 381° can be obtained.

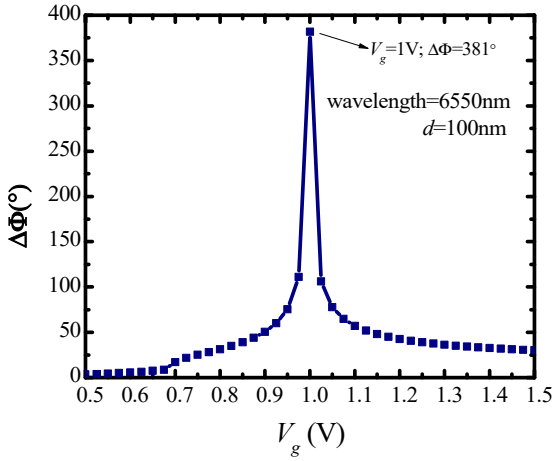

Figure 4. Dependence of phase shift on applied voltage. Incident wavelength is 6550 nm, dielectric material is $HfAlO_x$ and d = 100 nm.

To further confirm the theoretical results presented above, the phase modulation performance of the presented structure is simulated and verified using an RF module of COMSOL Multiphysics software. Here, the operating wavelength is 6550 nm with V_g fixed at 1 V and d fixed at 100 nm. The electric field distribution of the SPPs wave guided by the presented structure is shown in Figure 5a. It can be clearly observed that the SPPs wave is excited on the surface of graphene and dielectric medium. Figure 5b shows the phase shift in the SPPs wave in the direction of transmission. The phase shift comparison under different transmission lengths (L) is shown in Figure 5c. It can be concluded from the simulation results that the structure achieves 360-degree phase shift, which is consistent with the theoretical results.

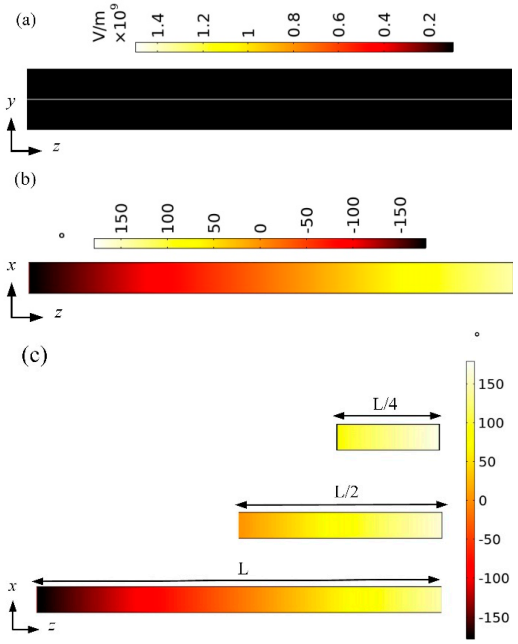

Figure 5. Simulation results of the proposed structure: (**a**) electric field distributions of SPPs guided by the proposed structure; (**b**) phase shift in the SPPs wave in the direction of transmission; (**c**) phase shift comparison of different transmission lengths.

In addition, the simulation comparison between $HfAlO_x$ and SiO_2 was carried out to demonstrate the superiority of $HfAlO_x$ as a dielectric material. Figure 6a,b shows the simulated tunable phase shift of mid-infrared with voltage variation. Figure 6c,d shows the dependence of phase shift on applied voltage at 6550 nm wavelength for different dielectric layer thicknesses. As revealed in Figure 6c,d, the depth of phase modulation and the best modulation voltage point are changed with different dielectric layer thicknesses (d). It can be observed clearly that $HfAlO_x$ has the obvious advantages of a low operating voltage compared with SiO_2. Besides this, excellent phase modulation property and perfect contact with graphene make $HfAlO_x$ the best choice for dielectric material [35].

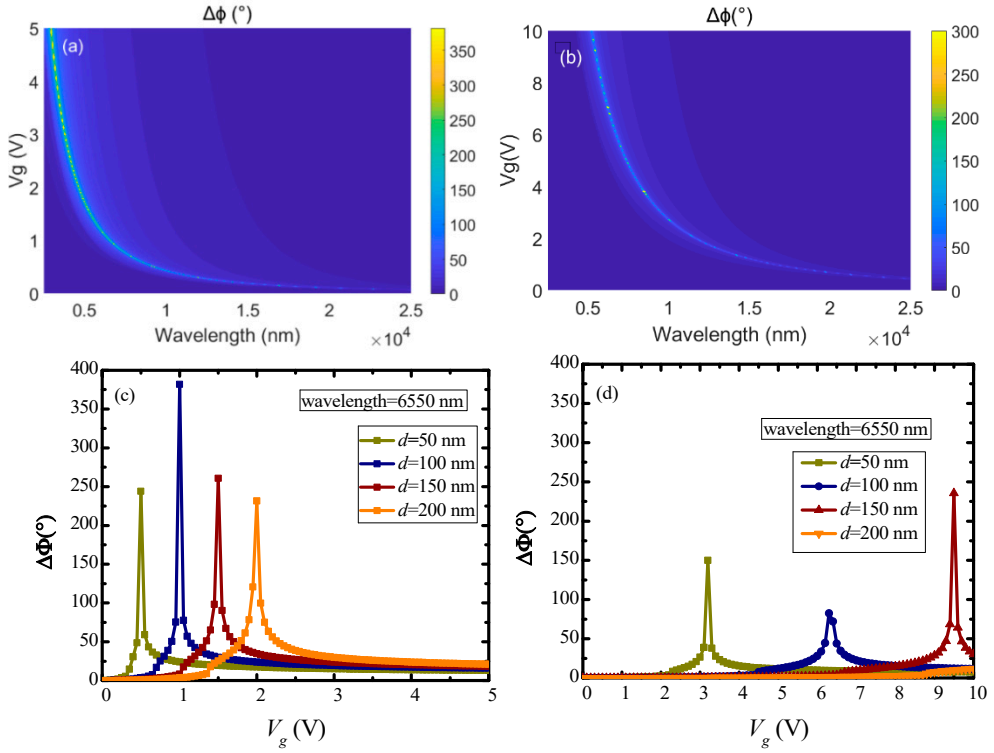

Figure 6. Comparison of phase modulation properties for different dielectric materials: (**a**) simulated tunable phase shift of mid-infrared with voltage variation for $HfAlO_x$ dielectric; (**b**) simulated tunable phase shift of mid-infrared with voltage variation for SiO_2 dielectric; (**c**) dependence of phase shift on applied voltage at 6550 nm for $HfAlO_x$ dielectric; (**d**) dependence of phase shift on applied voltage at 6550 nm for Si dielectric.

The dielectric constant of $HfAlO_x$ used in the previous simulations is 14.3. In order to prove that 14.3 is the optimal dielectric constant of $HfAlO_x$ under the design parameters of the presented structure, the influence of the dielectric constant of $HfAlO_x$ on the phase shift characteristics of the presented structure was discussed here. The value of the dielectric constant of $HfAlO_x$ is about between 9 and 20, which is dependent on the manufacturing process and the stoichiometric ratio of Hf, Al and O. Which dielectric constant is the optimal constant depends on other parameters, including applied voltage (V_g) and $HfAlO_x$ dielectric thickness (d), and the relationship between them is expressed by the formulas shown in the methods. In this simulation, we set the incident wavelength at 6550 nm. As revealed in Figure 7, phase shift is selective to the dielectric constant of $HfAlO_x$, and the dielectric constant of $HfAlO_x$ at the maximum phase shift point is different when given different V_g and d. This is mainly because the different graphene conductivity resulted from the different V_g and d. The maximum of phase shift shows nonlinear changes, which depends on the nonlinear relationship between V_g, ε_r and d. As revealed from Figure 7, 14.3 is the optimal dielectric constant of $HfAlO_x$ for the presented structure.

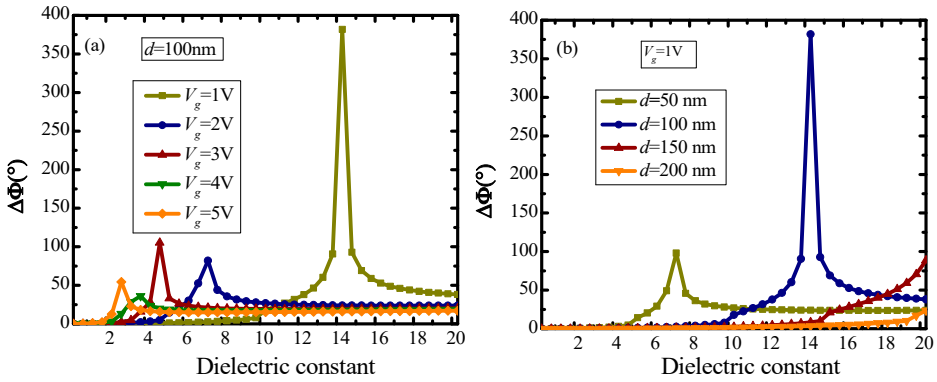

Figure 7. Dependence of the dielectric constant of $HfAlO_x$ on the phase shift: (**a**) given different v_g; (**b**) given different d.

5. Conclusions

In this paper, we investigate the phase modulation properties of graphene SPPs in detail. To numerically demonstrate the feasibility of graphene SPPs' phase modulation, a sandwich waveguide structure of dielectric–graphene–dielectric is presented here. It is found that this structure can realize the continuous tuning of the phase shift in mid-infrared, covering the phase range from 0° to 360°. Given $HfAlO_x$, the dielectric thickness of 100 nm and drive voltage of 1 V, the proposed structure can realize a phase shift of 381° at 6.55 um, where only an 800 nm optical path is needed. The results in this paper confirm the unique properties of graphene SPPs in phase modulation and demonstrate the great potential of graphene SPPs phase modulation in mid-infrared, which can be widely applied to the design of on-chip interferometers and tunable modulators.

Author Contributions: Conceptualization, Y.W., H.L. and S.W.; Data curation, M.C.; Investigation, H.Z. and Y.Q.; Writing—original draft, Y.W.; Writing—review & editing, H.L. and S.W. All authors have read and agreed to the published version of the manuscript.

Funding: This research is supported by the Foundation for Fundamental Research of China (Grant No. JSZL2016110B003), the Major Fundamental Research Program of Shaanxi (Grant No. 2017ZDJC-26), and innovation Foundation of Radiation Application (Grant No. KFZC2018040206).

Acknowledgments: We acknowledge the Foundation for Fundamental Research of China, the Major Fundamental Research Program of Shaanxi, innovation Foundation of Radiation Application, and the valuable suggestions from the peer reviewers.

Conflicts of Interest: The authors declare no conflict of interest.

References

1. Zayats, A.V.; Smolyaninov, I.I.; Maradudin, A.A. Nano-optics of surface plasmon polaritons. *Phys. Rep.* **2005**, *408*, 131–314. [CrossRef]
2. Butt, M.; Khonina, S.; Kazanskiy, N. Enhancement of evanescent field ratio in a silicon strip waveguide by incorporating a thin metal film. *Laser Phys.* **2019**, *29*, 076202. [CrossRef]
3. Butt, M.; Khonina, S.; Kazanskiy, N. Plasmonic refractive index sensor based on metal–insulator-metal waveguides with high sensitivity. *J. Mod. Opt.* **2019**, *66*, 1038–1043. [CrossRef]
4. Butt, M.; Khonina, S.; Kazanskiy, N. Hybrid plasmonic waveguide-assisted Metal–Insulator–Metal ring resonator for refractive index sensing. *J. Mod. Opt.* **2018**, *65*, 1135–1140. [CrossRef]
5. Zhernovnykova, O.A.; Popova, O.; Deynychenko, G.; Deynichenko, T.; Bludov, Y. Surface plasmon-polaritons in graphene, embedded into medium with gain and losses. *J. Phys. Condens. Matter.* **2019**, *31*, 465301. [CrossRef]
6. Su, Y.; Lin, Q.; Zhai, X.; Wang, L.-L. Enhanced Confinement of Terahertz Surface Plasmon Polaritons in Bulk Dirac Semimetal-Insulator-Metal Waveguides. *Nanoscale Res. Lett.* **2018**, *13*, 308. [CrossRef]
7. Chau, Y.-F.; Lin, Y.-J.; Tsai, D.P. Enhanced surface plasmon resonance based on the silver nanoshells connected by the nanobars. *Opt. Express* **2010**, *18*, 3510–3518. [CrossRef]

8. Chau, Y.-F.; Yeh, H.-H.; Liao, C.-C.; Ho, H.-F.; Liu, C.-Y.; Tsai, D.P. Controlling surface plasmon of several pair arrays of silver-shell nanocylinders. *Appl. Opt.* **2010**, *49*, 1163–1169. [CrossRef]
9. Wang, Y.; Wang, S.; Cai, M.; Liu, H. A Long Propagation Distance Hybrid Triangular Prism Waveguide for Ultradeep Subwavelength Confinement. *IEEE Sens. J.* **2019**, *19*, 11159–11166. [CrossRef]
10. Wang, Y.; Liu, H.; Wang, S.; Cai, M.; Ma, L. Optical Transport Properties of Graphene Surface Plasmon Polaritons in Mid-Infrared Band. *Crystals* **2019**, *9*, 354. [CrossRef]
11. Lu, F.; Liu, B.; Shen, S. Infrared wavefront control based on graphene metasurfaces. *Adv. Opt. Mater.* **2014**, *2*, 794–799. [CrossRef]
12. Koppens, F.H.; Chang, D.E.; de Abajo, F.J.G. Graphene plasmonics: A platform for strong light–matter interactions. *Nano Lett.* **2011**, *11*, 3370–3377. [CrossRef] [PubMed]
13. Jablan, M.; Buljan, H.; Soljačić, M. Plasmonics in graphene at infrared frequencies. *Phys. Rev. B* **2009**, *80*, 245435. [CrossRef]
14. Rosa, H.G.; Steinberg, D.; Zapata, J.D.; Saito, L.A.M.; Cárdenas, A.M.; Gomes, J.C.V.; Souza, E.A.T.D. Raman Mapping Characterization of All-Fiber CVD Monolayer Graphene Saturable Absorbers for Erbium-Doped Fiber Laser Mode Locking. *J. Lightwave Technol.* **2015**, *33*, 4118–4123. [CrossRef]
15. Fei, Z.; Andreev, G.O.; Bao, W.; Zhang, L.M.; McLeod, A.S.; Wang, C.; Stewart, M.K.; Zhao, Z.; Dominguez, G.; Thiemens, M. Infrared nanoscopy of Dirac plasmons at the graphene–SiO2 interface. *Nano Lett.* **2011**, *11*, 4701–4705. [CrossRef] [PubMed]
16. Kuzmin, D.A.; Bychkov, I.V.; Shavrov, V.G.; Temnov, V.V. Plasmonics of magnetic and topological graphene-based nanostructures. *Nanophotonics* **2018**, *7*, 597–611. [CrossRef]
17. Xu, Z.; Wu, D.; Liu, Y.; Liu, C.; Yu, Z.; Yu, L.; Ye, H. Design of a tunable ultra-broadband terahertz absorber based on multiple layers of graphene ribbons. *Nanoscale Res. Lett.* **2018**, *13*, 143. [CrossRef]
18. Shan, Y.; Tang, J.; Wu, L.; Lu, S.; Dai, X.; Xiang, Y. Spatial self-phase modulation and all-optical switching of graphene oxide dispersions. *J. Alloys.* **2019**, *771*, 900–904. [CrossRef]
19. Kats, M.A.; Blanchard, R.; Genevet, P.; Yang, Z.; Qazilbash, M.M.; Basov, D.; Ramanathan, S.; Capasso, F. Thermal tuning of mid-infrared plasmonic antenna arrays using a phase change material. *Opt. Lett.* **2013**, *38*, 368–370. [CrossRef]
20. Samolis, P.D.; Sander, M. Phase-sensitive lock-in detection for high-contrast mid-infrared photothermal imaging with sub-diffraction limited resolution. *Opt. Express* **2019**, *27*, 2643–2655. [CrossRef]
21. Sherrott, M.C.; Hon, P.W.; Fountaine, K.T.; Garcia, J.C.; Ponti, S.M.; Brar, V.W.; Sweatlock, L.A.; Atwater, H.A. Experimental demonstration of> 230 phase modulation in gate-tunable graphene–gold reconfigurable mid-infrared metasurfaces. *Nano Lett.* **2017**, *17*, 3027–3034. [CrossRef] [PubMed]
22. Ying, D.; Xie, T.; Wang, Z.; Liu, Q.; Ye, K.; Jin, Z. A closed-loop RFOG based on digital serrodyne and sine modulations with two LiNbO3 phase modulators. *Opt. Commun.* **2019**, *452*, 151–157. [CrossRef]
23. Herzog, B.; Lingnau, B.; Kolarczik, M.; Helmrich, S.; Lüdge, K.; Woggon, U.; Owschimikow, N. Role of Mixed-dimensional Excitons in the Phase Dynamics of Semiconductor Optical Lasers and Amplifiers. In Proceedings of the CLEO: QELS Fundamental Science, (Optical Society of America, 2019), JW2A. 24, San Jose, CA, USA, 5–10 May 2019.
24. Fei, Z.; Rodin, A.; Andreev, G.O.; Bao, W.; McLeod, A.; Wagner, M.; Zhang, L.; Zhao, Z.; Thiemens, M.; Dominguez, G. Gate-tuning of graphene plasmons revealed by infrared nano-imaging. *Nature* **2012**, *487*, 82. [CrossRef] [PubMed]
25. Li, Z.; Henriksen, E.A.; Jiang, Z.; Hao, Z.; Martin, M.C.; Kim, P.; Stormer, H.; Basov, D.N. Dirac charge dynamics in graphene by infrared spectroscopy. *Nat. Phys.* **2008**, *4*, 532. [CrossRef]
26. Fang, Z.; Thongrattanasiri, S.; Schlather, A.; Liu, Z.; Ma, L.; Wang, Y.; Ajayan, P.M.; Nordlander, P.; Halas, N.J.; de Abajo, F.J.G. Gated tunability and hybridization of localized plasmons in nanostructured graphene. *ACS Nano* **2013**, *7*, 2388–2395. [CrossRef] [PubMed]
27. Jadidi, M.M.; Sushkov, A.B.; Myers-Ward, R.L.; Boyd, A.K.; Daniels, K.M.; Gaskill, D.K.; Fuhrer, M.S.; Drew, H.D.; Murphy, T.E. Tunable terahertz hybrid metal–graphene plasmons. *Nano Lett.* **2015**, *15*, 7099–7104. [CrossRef]
28. Wang, X.; Meng, H.; Deng, S.; Lao, C.; Wei, Z.; Wang, F.; Tan, C.; Huang, X. Hybrid Metal Graphene-Based Tunable Plasmon-Induced Transparency in Terahertz Metasurface. *Nanomaterials* **2019**, *9*, 385. [CrossRef]
29. Mueller, T.; Xia, F.; Freitag, M.; Tsang, J.; Avouris, P. Role of contacts in graphene transistors: A scanning photocurrent study. *Phys. Rev. B* **2009**, *79*, 245430. [CrossRef]

30. Goldflam, M.D.; Ruiz, I.; Howell, S.W.; Wendt, J.R.; Sinclair, M.B.; Peters, D.W.; Beechem, T.E. Tunable dual-band graphene-based infrared reflectance filter. *Opt. Express* **2018**, *26*, 8532–8541. [CrossRef]
31. Casiraghi, C.; Pisana, S.; Novoselov, K.; Geim, A.; Ferrari, A. Raman fingerprint of charged impurities in graphene. *Appl. Phys. Lett.* **2007**, *91*, 233108. [CrossRef]
32. Qu, S.; Ma, C.; Liu, H. Tunable graphene-based hybrid plasmonic modulators for subwavelength confinement. *Sci. Rep.* **2017**, *7*, 1–8. [CrossRef] [PubMed]
33. Fowler, J.D.; Allen, M.J.; Tung, V.C.; Yang, Y.; Kaner, R.B.; Weiller, B.H. Practical chemical sensors from chemically derived graphene. *ACS Nano* **2009**, *3*, 301–306. [CrossRef] [PubMed]
34. Yota, J.; Shen, H.; Ramanathan, R. Characterization of atomic layer deposition HfO_2, Al_2O_3, and plasma-enhanced chemical vapor deposition Si_3N_4 as metal–insulator–metal capacitor dielectric for GaAs HBT technology. *J. Vac. Sci. Technol. A Vac. Surf.* **2013**, *31*, 01A134. [CrossRef]
35. Zheng, L.; Cheng, X.; Cao, D.; Wang, Z.; Xu, D.; Xia, C.; Shen, L.; Yu, Y. Effects of rapid thermal annealing on properties of HfAlO films directly deposited by ALD on graphene. *Mater. Lett.* **2014**, *137*, 200–202. [CrossRef]
36. Christensen, J.; Manjavacas, A.; Thongrattanasiri, S.; Koppens, F.H.; de Abajo, F.J.G. Graphene plasmon waveguiding and hybridization in individual and paired nanoribbons. *ACS Nano* **2011**, *6*, 431–440. [CrossRef]
37. Cai, M.; Wang, S.; Gao, B.; Wang, Y.; Han, T.; Liu, H. A New Electro-Optical Switch Modulator Based on the Surface Plasmon Polaritons of Graphene in Mid-Infrared Band. *Sensors* **2019**, *19*, 89. [CrossRef]
38. Totsuka, K.; Kobayashi, N.; Tomita, M. Slow Light in Coupled-Resonator-Induced Transparency. *Phys. Rev. Lett.* **2007**, *98*, 213904. [CrossRef]
39. Kischkat, J.; Peters, S.; Gruska, B.; Semtsiv, M.; Chashnikova, M.; Klinkmüller, M.; Fedosenko, O.; Machulik, S.; Aleksandrova, A.; Monastyrskyi, G. Mid-infrared optical properties of thin films of aluminum oxide, titanium dioxide, silicon dioxide, aluminum nitride, and silicon nitride. *Appl. Opt.* **2012**, *51*, 6789–6798. [CrossRef]
40. Li, C.; Xiao, Z.; Li, W.; Zou, H. Tunable multiband band-stop filter based on graphene metamaterial in THz frequency. *J. Electromagn. Waves* **2018**, *32*, 2481–2489. [CrossRef]
41. Wang, X.; Meng, H.; Liu, S.; Deng, S.; Jiao, T.; Wei, Z.; Wang, F.; Tan, C.; Huang, X. Tunable graphene-based mid-infrared plasmonic multispectral and narrow band-stop filter. *Mater. Res. Express* **2018**, *5*, 045804. [CrossRef]
42. Ristić, S.; Prijić, A.; Prijić, Z. Dependence of static dielectric constant of silicon on resistivity at room temperature. *Serb. J. Electr. Eng.* **2004**, *1*, 237–247. [CrossRef]